Structural Evolution and Catalytic Properties of Nanostructured Cu/ZrO_2 Catalysts Prepared by Oxalate Gel-Coprecipitation Technique

Lu-Cun Wang, Qian Liu, Miao Chen, Yong-Mei Liu, Yong Cao,* He-Yong He, and Kang-Nian Fan

Department of Chemistry & Shanghai Key Laboratory of Molecular Catalysis and Innovative Materials, Fudan University, Shanghai 200433, People's Republic of China

Received: July 26, 2007; In Final Form: September 4, 2007

A series of zirconia-supported copper oxide catalysts synthesized by decomposition of the oxalate precursors formed by oxalate gel-coprecipitation in alcoholic solution were extensively investigated in relation to their performance in methanol steam reforming. The combination of different techniques (N_2 adsorption, X-ray diffraction (XRD), N_2O titration, H_2-TPR, diffuse reflectance Fourier transform infrared, Raman, and X-ray photoelectron spectroscopy) in the characterization of Cu/ZrO_2 catalysts shows that the surface and structural characteristics of the zirconia phase as well as the dispersion and nature of the copper species depend strongly on the calcination temperature. Temperature-programmed reduction patterns reveal the presence of three types of copper species on the ZrO_2 support. XRD results indicate that, depending on the calcination temperature, a substantial incorporation of Cu species into the zirconia lattice leading to a strong $Cu-ZrO_2$ metal−support interaction may occur. The N_2O titration reveals that the 550 °C calcined material exhibits the highest metallic copper surface area as compared to other samples, as opposed to in situ XRD analysis showing that the lower the calcination temperature the higher the copper dispersion. Spectroscopic measurements reveal that the phase transformation of zirconia from tetragonal to monoclinic takes place initially at the surface regions of the $Cu-ZrO_2$ sample, as evidenced from the fact that the monoclinic phase can be detected first by Raman spectroscopies for the samples calcined at a lower temperature than by XRD. The highest activity was achieved for the 550 °C calcined material, illustrating that the creation of monoclinic phase enriched on the surface of tetragonal zirconia in Cu/ZrO_2 are beneficial for the generation of copper catalyst with enhanced activities.

1. Introduction

Copper-containing catalysts have been extensively employed in the past decades for the selective catalytic reduction of NO_x, water gas shift reaction, synthesis and steam-reforming of methanol.[1−11] It is also established that copper catalysts are very selective for a number of hydrogenation and dehydrogenation reactions, such as conversion of furfural to furfuryl alcohol, methyl ester to methyl alcohol, or the transformation of alcohols into their corresponding aldehydes or ketones.[12−16] For most of these reactions, the nature of the supported oxide and the dispersion of active component are thought to be most relevant to understanding the catalytic properties of the systems.[5] Zirconia has recently emerged as a particularly interesting support material.[5,17−20] ZrO_2 presents special characteristics such as high fracture toughness, ionic conductivity, and stability even under reducing conditions. Moreover, the possession of both amphoteric and redox functions makes it appealing as a more suitable carrier for a number of catalytic applications.[20] As a result, the use of zirconia other than silica or alumina as a promoter or more frequently a support material has attracted considerable interest in recent years.[21] In CO or CO_2 hydrogenation for instance, zirconia addition to Cu/SiO_2 or Cu/ZnO catalysts leads to improved long-term stability as well as both enhanced activity/selectivity toward alcohol.[22−31] It is also revealed that Cu/ZrO_2 catalysts exhibited superior activity when compared to the conventional Cu/ZnO catalysts for the steam reforming of methanol.[32−35]

Due to its fundamental and ever increasing importance, intensive recent studies have been carried out to understand the synergetic interaction between copper and zirconia. In particular, it has been found that the activity of the Cu/ZrO_2 catalysts is critically dependent on the phase structure of ZrO_2.[36−40] Within this context, Jung and Bell have reported that Cu/ZrO_2 catalysts prepared with monoclinic ZrO_2 (m-ZrO_2) are nearly an order of magnitude more active for methanol synthesis and exhibit higher methanol selectivities than catalysts with the same Cu surface density deposited on tetragonal ZrO_2 (t-ZrO_2) with the same surface area as m-ZrO_2.[36] The origin of these differences has been explained by the presence of higher concentration of anionic defects on m-ZrO_2 than t-ZrO_2.[37,38] The effects of the zirconia phase have also been noted in studies of the steam reforming of methanol, where maintaining the amorphous nature of zirconia under calcination and reaction conditions as well as a high-copper/zirconia interfacial area has been considered the key aspect for obtaining highly active and selective copper catalysts with improved stability.[41] Given the role of Cu as the active component for methanol synthesis or related processes, the surface area of Cu is also expected to play a vital role in these catalytic systems.[42,43] This is supported by, in general terms, a linear correlation between metallic Cu surface area and the activity of the catalyst.[38,39]

Among the three main kinds of crystalline ZrO_2, that is, tetragonal (t-ZrO_2), monoclinic (m-ZrO_2), and cubic (c-ZrO_2),

* To whom correspondence should be addressed. E-mail: yongcao@fudan.edu.cn.

10.1021/jp075930k CCC: $37.00
Published on Web 10/10/2007

the catalytic study of c-ZrO_2 is rarely addressed, partly due to its lack of stability at ambient conditions.[44] In both cubic and tetragonal phases, the coordination of Zr is 8-fold with oxygen anions forming two jointed tetrahedra, and the oxygen atom is shared by four adjacent Zr atoms. However, distortions of the tetrahedra in these two phases lead to crystallographic differences and result in the different arrangement of the Zr−O and Zr−OH bonds on the surface of their particles. The distortion of the [ZrO_8] unit is greater in t-ZrO_2 than in c-ZrO_2 in which four Zr−O bonds in the elongated tetrahedron are longer than the four Zr−O bonds associated with the flattened tetrahedron. In m-ZrO_2, the coordination of Zr is 7-fold with oxygen anions forming two types of nonequivalent oxygen sites.[45] The structural distortion of the [ZrO_7] unit in m-ZrO_2 is the greatest among the three allotropic phases, having seven different Zr−O bond lengths.[45] The different spacing and symmetry of these Zr−O and −OH bonds on the surface of the particles of t-ZrO_2 and m-ZrO_2 are considered to play key roles in determining the dispersion of the active metal component and hence the catalytic properties of the Cu/ZrO_2 material.[38,40] However, a fundamental understanding of the structural distribution in relation to catalytic evolution of a Cu−ZrO_2 system, in particular the material obtained by liquid coprecipitation pathway, is to the best of our knowledge still lacking.

In the present investigation, we report the characterization of Cu/ZrO_2 catalysts prepared by decomposition of oxalate precursors formed by oxalate gel-coprecipitation (OGC) of metal nitrates in alcoholic solution.[46] Very recently, we have shown that the OGC technique can allow the fabrication of a new type of nanostructured Cu/ZrO_2 materials featured with a high component dispersion thus being highly effective for methanol steam reforming.[47] Given the calcination process frequently employed as the key step in preparation of a copper catalyst, the present work aims to identify the surface and structural evolution occurring in these nanostructured catalyst systems as a function of precursor calcination. To gain an insight into the respective nature of Cu and ZrO_2 phases as well as the structural properties of the Cu/ZrO_2 catalyst in relation to their performance in methanol steam reforming, extensive characterization by N_2 adsorption, X-ray diffraction (XRD), temperature-programmed reduction (TPR), N_2O titration, X-ray photoelectron spectroscopy (XPS), diffuse reflectance Fourier transform infrared (DRIFTS) and Raman spectroscopies has been carried out.

2. Experimental Section

2.1. Catalyst Preparation. Cu/ZrO_2 catalysts with Cu/Zr ratio of 1/2 were prepared by oxalate gel-coprecipitation method. An alcoholic solution of 20% excess of oxalic acid was injected rapidly into a mixed alcoholic solution (each 0.1 M) of copper nitrate and zirconium nitrate at room temperature under vigorous stirring. The resultant gel-like precipitates were separated by centrifuge followed by drying at 110 °C overnight. Finally, calcination of the as-obtained materials was performed in a muffle oven at elevated temperatures ranging from 350 to 750 °C for 4 h. The as-prepared CuO−ZrO_2 mixed oxide samples were designated as CZ-*T*, where *T* denotes the calcination temperature.

2.2. Catalyst Characterization. The Brunauer−Emmet−Teller (BET) specific surface areas of the calcined catalysts were determined by adsorption−desorption of nitrogen at liquid nitrogen temperature, using a Micromeritics TriStar 3000 equipment. Sample degassing was carried out at 300 °C prior to acquiring the adsorption isotherm.

The X-ray powder diffraction (XRD) of the samples was carried out on a Germany Bruker D8Advance X-ray diffractometer using nickel-filtered Cu Kα radiation with a scanning angle (2θ) of 20−80°, a scanning speed of 2° min^{-1}, and a voltage and current of 40 kV and 40 mA, respectively. In situ XRD experiments performed are as follows: reduction of the calcined Cu/ZrO_2 oxide precursors in 5 vol % H_2 in argon in a temperature range from room temperature to 250 °C at a heating ramp of 1 °C min^{-1} was carried out in a XRK-900 high-temperature cell. In situ XRD patterns were recorded at 250 °C under simulated methanol steam-reforming conditions (c(MeOH) ∼ 5 vol %, c(H_2O) ∼6.5 vol % in 100 mL min^{-1} Ar) (20∼80° 2θ, step width 0.02° 2θ, counting time: 1s/dp (dp = data point)). The percentage of monoclinic phase (M%) in the oxide "support" was measured according to the equation:[48] $M\% = I_{M(\bar{1}11)}/(1.6I_{M(\bar{1}11)} + I_{T(111)})$, where $I_{M(\bar{1}11)}$ and $I_{T(111)}$ are the diffraction intensities of the monoclinic ($\bar{1}11$) ($2\theta = 30.4°$) and tetragonal (111) ($2\theta = 28.5°$) planes, respectively. The crystallite size corresponding to the broadening of each *hkl* line was determined from Sherrer equation: $d = k\lambda/\beta \cos\theta$, where $k = 0.89$, and $\lambda = 1.5406$ Å.

The DRIFT spectra were recorded using Bruker Vector 22 FT-IR spectrometer equipped with Spectra-Tech Diffuse Reflectance Accessory and a high-temperature in situ cell with ZnSe windows. A KBr beam splitter has been used with a DTGS detector. The catalyst was prereduced in situ at 300 °C for 4 h under atmospheric pressure by a stream of H_2. After switching to He, the sample was cooled down to 373 K, and CO was introduced for 15 min. Thereafter, the system was cooled to room temperature, swept with argon (99.99%), and the IR spectra was collected.

The specific surface area of metallic copper was measured by the adsorption and decomposition of N_2O on the surface of metallic copper as follows: $2Cu_{(s)} + N_2O \rightarrow N_2 + Cu_2O_{(s)}$. The pulse titration technique was employed. Pure nitrogen was used as the carrier gas and a thermal conduct detector was used to detect the amount of the consumption of N_2O.[49] The specific area of metallic copper was calculated from the total amount of N_2O consumption with 1.46×10^{19} copper atoms per m^2.[50]

TPR profiles were obtained on a homemade apparatus as described elsewhere.[46] Approximate 20 mg of a freshly calcined catalyst was placed on top of glass wool in a quartz reactor. TPR experiments were carried out in 5% H_2/Ar flowing at 40 mL min^{-1} with a ramping rate of 10 °C min^{-1} to a final temperature of 500 °C. The H_2 consumption was monitored using a thermal conductivity detector (TCD).

The laser Raman spectra were obtained at room temperature using a confocal microprobe Jobin Yvon Lab Ram Infinity Raman system with a spectral resolution of 2 cm^{-1}. The internal 514.5 nm line from Ar^+ excitation with a power of 10 mW was used as the source. The Raman signal was collected with a 90°-geometry.

XPS spectra were recorded with a Perkin-Elmer PHI 5000C system equipped with a hemispherical electron energy analyzer. The Mg Kα ($h\nu = 1253.6$ eV) was operated at 15 kV and 20 mA. The Cu 2p and Zr 3d core-level spectra were recorded and the corresponding binding energies (BE) were calibrated with respect to the C 1s line at 284.6 eV (accuracy within ± 0.2 eV). The background pressure during the data acquisition was kept below 2×10^{-9} Torr.

2.3. Catalytic Activity Tests. The catalytic test was conducted using a fixed-bed microreactor from 160 to 300 °C under atmospheric pressure. A 0.5 g catalyst diluted with 0.5 g quartz sand (both in 40−60 mesh) was packed in a stainless steel

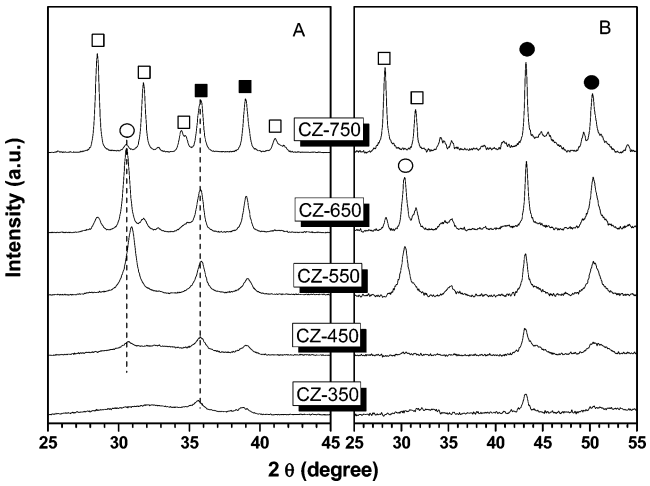

Figure 1. X-ray powder diffraction patterns of the CZ catalysts after calcination (A) and after exposure to reaction conditions (B). (□) m-ZrO_2, (○) t′-ZrO_2, (■) CuO, (●) Cu.

tubular reactor (6 mm i.d.). After reduction in a H_2/Ar (5/95) flowing of 60 mL min^{-1} at 250 °C for 6 h, premixed water and methanol with a H_2O/MeOH molar ratio of 1.3 at a flow rate of 44.0 mL-NTP min^{-1} were fed into the preheater maintained at about 250 °C by means of a microfeeder. The vaporized feed entered the reactor with a stream of Ar gas, which had a flow rate of 20 mL min^{-1} and then began the SRM reaction at the designated reaction temperature. The reaction products were first passed through a cold trap, then the gaseous products such as H_2, CO, CO_2, CH_4 were detected on-line by the gas chromatograph (Type GC-122, Shanghai Analysis) equipped with TCD and TDX-01 column; the liquid products, such as water and methanol, were analyzed by the same gas chromatograph equipped with another TCD detector and Porapak-Q column. Unless otherwise mentioned, the catalytic activity was evaluated from the data collected after 6 h of the on-stream operation by methanol conversion (X_{MeOH}), CO_2 selectivity (S_{CO2}), and CO selectivity (S_{CO}) in the outlet.

3. Results and Discussion

3.1. Textural and Structural Evolution. Figure 1A compares the XRD patterns of calcined catalysts obtained by decomposition of oxalate precursors formed by oxalate gel-coprecipitation of metal nitrates in alcoholic solution. Upon calcination at elevated temperatures from 350 to 750 °C, a progressive enhancement of the crystallite size of the CuO phase is identified, as reflected from a continuous sharpening and intensification of the diffraction peaks for the calcined samples as shown in Figure 1. It is interesting to note that a significantly different variation behavior of the structural evolution as a function of the precursor calcination has been observed in the zirconia phase. As shown in Figure 1A, only weak and broad diffraction peaks of CuO can be observed for the catalyst calcined at 350 °C, pointing to an amorphous or semicrystalline nature of the zirconia in CZ-350 sample. When the temperature was increased to 450 °C, the diffraction peaks of metastable tetragonal ZrO_2 phase (t-ZrO_2) appeared, the intensity of which increased drastically as the temperature reached 550 °C. Notice that the t-ZrO_2 peak at $2\theta = 30.6°$ shifted to higher angle upon calcination at 550 °C, indicating a substantial incorporation of Cu^{2+} ions into the zirconia lattice (i.e., they occupy the position of the Zr).[51] After a progressive calcination at 650 °C, partial transformation from tetragonal to monoclinic phase occurred (m-ZrO_2, ca. 32%), where the reshift of the t-ZrO_2 peak to a lower angle could be due to a phase segregation of CuO accompanied with the zirconia phase transformation.[51] Further calcination at 750 °C results in the nearly total replacement of tetragonal by monoclinic phase for the ZrO_2 phase.

To investigate the active phase of the Cu/ZrO_2 catalysts, the XRD patterns of the five catalysts after reduction followed by subsequent reaction at 250 °C were collected and are shown in Figure 1B. For all the catalysts, besides the diffraction features corresponding to zirconia phase only diffraction peaks characteristic of metallic copper can be observed, indicating that the bulk CuO in the catalysts was reduced to Cu^0 and the main active phase of the Cu/ZrO_2 catalyst is metallic copper.[47] Assuming that Cu particles were spherical, the average copper metal crystallite sizes were calculated from the full width at half-maximum (FWHM) of Cu (111) diffraction lines. The calculation results as shown in Table 1 reveal a much smaller copper particle size for CZ-350 (12.1 nm), CZ-450 (13.2 nm), and CZ-550 (14.7 nm) samples as compared to CZ-650 (21.3 nm) and CZ-750 (24.0 nm). The variation of ZrO_2 phase is similar to that in the oxide precursors; the only difference is that the proportion of m-ZrO_2 phase in the high-temperature calcined samples increased under reaction conditions, from ca. 32 to 48% for CZ-650 and from ca. 96 to 100% for CZ-750.

The physicochemical properties of the various CZ catalysts obtained by calcination at different temperatures are also presented in Table 1. With increasing calcination temperature from 350 to 750 °C, the BET surface areas of the Cu/ZrO_2 catalysts decreased monotonically from 63 to 8 $m^2\ g^{-1}$. The effect of the calcination temperature on specific surface area for the present as-synthesized sample is dramatic as reported for conventional aqueous coprecipitation-derived Cu/ZrO_2 materials in the literature.[52] By using a quasi-sphere model, the copper metal surface area was estimated by the crystallite size determined by the in situ XRD results.[52] Notice that the "XRD surface areas" (S_{Cu}^{XRD}) exhibited a similar variation trend with respect to the BET surface area, from 18.9 to 9.5 $m^2\ g_{cat}^{-1}$, showing that the higher the calcination temperature is, the lower the copper dispersion is. At this situation, it is interesting to note that the data of the metallic Cu surface area as measured by N_2O titration demonstrate clearly that the 550 °C calcined catalyst exhibits the highest copper dispersion as compared to other samples, inferring a unique $Cu-ZrO_2$ metal−support interaction in this material. Moreover, it is noticed that for all the samples the S_{Cu}^{XRD} values are always much higher than the S_{Cu}^{N2O} values. These discrepancies may be caused by agglomeration of Cu particles or a strong $Cu-ZrO_2$ metal support interaction that reduces the accessible Cu surface area.

Raman spectroscopy is an effective technique to study the surface characteristics of the catalysts. Figure 2 shows the visible Raman spectra of Cu/ZrO_2 samples calcined at different temperatures. The samples CZ-350 and CZ-450 exhibit essentially the same Raman features in which relatively weak and broad bands located at 144, 270, 322, 435, 598, and 630 cm^{-1} can be identified. According to the literature,[54] the bands at 144, 435, 598, and 630 cm^{-1} can be assigned to tetragonal ZrO_2, while the bands at 270 and 322 cm^{-1} are characteristic of CuO. The absence of sharp bands in the spectra obtained by calcination at lower temperatures indicates the semicrystalline nature of the low-temperature calcined samples, which is in good accordance with the XRD results. With increasing calcination temperature to 550 °C, new bands at 174, 210, 324, 366, 465, 522, and 548 cm^{-1}, all characteristic of well-defined monoclinic ZrO_2, are observed. Coupled with the XRD data and previous observations for pure zirconia phase transformation,[54] this

TABLE 1: Physicochemical Properties of Cu/ZrO2 Catalysts Calcined at Different Temperatures

sample	S_{BET} (m^2/g)	V_{pore} (cm^3/g)	$S_{Cu}{}^{N_2O}$ [a] ($m^2/gcat$)	$S_{Cu}{}^{XRD}$ [b] ($m^2/gcat$)	d_{CuO} [c] (nm)	d_{ZrO2} [c,e] (nm)	ZrO_2 phase [c,f] (%)	d_{Cu} [d] (nm)	d_{ZrO2} [d,e] (nm)	ZrO_2 phase [d,f] (%)
CZ-350	63	0.25	4.0	18.9	8.8	[g]		12.1	−	
CZ-450	58	0.23	5.9	17.3	9.5			13.2	−	
CZ-550	43	0.19	8.7	15.6	10.6	T10.4	T100	14.7	T8.3	T100
CZ-650	21	0.13	4.8	10.7	16.5	M9.8/T14.0	M32/T68	21.3	M15.2/T13.2	M48/T52
CZ-750	8	0.07	2.4	6.5	19.9	M22.0/T16.9	M96/T4	24.0	M23	M100

[a] Cu metal surface area determined by N_2O decomposition method. [b]Cu metal surface area estimated by the in situ XRD crystallite size. [c]Determined for the working catalyst by the XRD data of oxide precursors. [d]Determined for the working catalyst by the in situ XRD data. [e]Average crystal size obtained with the Scherrer equation by using the $(\bar{1}11)$ diffraction ($2\theta = 28.5°$) for monoclinic and the (111) diffraction ($2\theta = 30.4°$) for tetragonal crystals; M and T represent the monoclinic and tetragonal phase, respectively. [f]Percentage of monoclinic phase $= I_{M(\bar{1}11)}/(1.6I_{M(\bar{1}11)} + I_{T(111)})$. [g]Not determined.

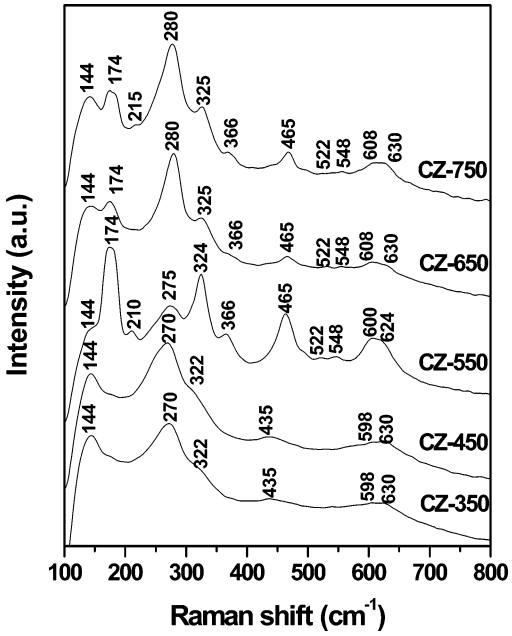

Figure 2. Raman spectra of various CuO/ZrO_2 catalysts.

indicates that the phase transformation of zirconia from tetragonal to monoclinic occurs already on the surface region of the 500 °C calcined Cu/ZrO_2 material. Further calcination at 650 and 750 °C results in appreciable attenuation of these bands. Note that the band at 270 cm^{-1} due to CuO in the samples CZ-350 and CZ-450 shifted to 280 cm^{-1} in CZ-650 and became sharper, indicating the increase of the CuO particle size.[55]

3.2. Chemical State and Redox Properties. The catalyst surface composition and oxidation state were investigated by XPS. Figures 3and 4 show Zr 3d and Cu 2p XPS of various CuO/ZrO_2 calcined catalysts, respectively. The Zr $3d_{5/2}$ and Zr $3d_{3/2}$ binding energy values are in the range of 179.8 and 184.5 eV, respectively. The binding energies of Zr $3d_{5/2}$ and its FWHM values are reported in Table 2. The FWHM values for samples CZ-350 and CZ-450 are found to be around 2.43, implying that only one type of doublet is present. This, together with the binding energy value of ca. 182.0 eV measured for Zr $3d_{5/2}$, is indicative the presence of a single type of zirconium oxide with an oxidation state of +4.[56] After calcination at temperatures above 550 °C, the spectra exhibit a wide peak width consisting of two doublets with Zr $3d_{5/2}$ binding energies at about 180.0 and 182.0 eV. As shown in the fitting to these curves, the lower BE values of the additional Zr species are attributable to the formation of surface zirconium sites having relatively higher electron density. Similar effect has been previously observed in the case of $Fe(NO_3)_2$ impregnated ZrO_2[56] and $Cu/ZnO/ZrO_2$ catalysts.[57] It was reported that oxygen coordinatively unsaturated Zr sites such as Zr^{3+} centers on ZrO_2 surface were

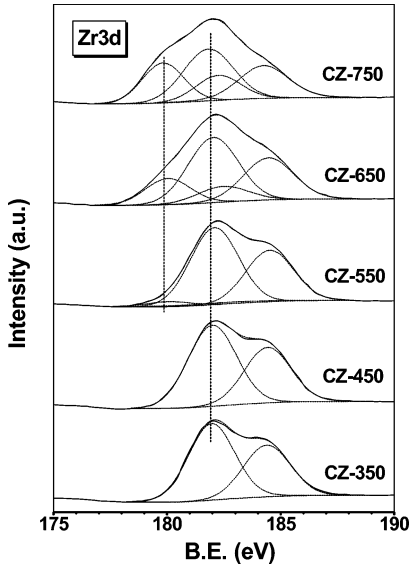

Figure 3. Zr 3d XPS spectra of various CuO/ZrO_2 catalysts.

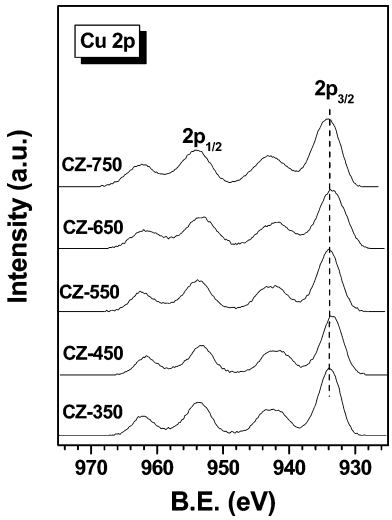

Figure 4. Cu 2p XPS spectra of various CuO/ZrO_2 catalysts.

detected upon calcination in air at temperatures higher than 500 °C, accompanied with the formation of oxygen vacancies in the ZrO_2 lattice.[56,57] Also in this case, in line with the formation of monoclinic-enriched zirconia on the surface region of the calcined materials, the low BE Zr species evidenced in the above 550 °C calcined Cu/ZrO_2 samples may be associated with the oxygen vacancies on the surface or subsurface of ZrO_2 lattice.

From Figure 4, it can be seen that all the catalysts exhibit Cu $2p_{3/2}$ main peaks at about 933.6 eV accompanied by intense shakeup satellite peaks at about 942 eV, respectively, which suggests the main copper oxidation state as +2.[57] As the

TABLE 2: XPS Results of Cu/ZrO_2 Catalysts Calcined at Different Temperatures

sample	BE and FWHM of $Cu2p_{3/2}$ (eV)	fraction of Cu species (%)	BE and FWHM of $Zr3d_{5/2}$ (eV)	fraction of Zr species (%)	Cu/Zr molar ratio
CuZr-350	933.9 (3.7)	100	182.0 (2.4)	100	0.33
CuZr-450	934.1 (3.8)	100	182.0 (2.5)	100	0.37
CuZr-550	934.0 (3.8)	87.3	182.1 (2.5)	94.6	0.56
	931.8 (3.7)	12.7	180.1 (2.3)	5.4	
CuZr-650	934.2 (3.8)	47.7	182.0 (2.6)	73.4	0.47
	932.0 (3.7)	52.3	180.0 (2.4)	26.6	
CuZr-750	934.1 (3.8)	37.1	181.8 (2.6)	60.7	0.42
	932.1 (3.7)	62.9	179.8 (2.2)	39.3	

calcination temperature increased above 550 °C, a shift toward lower binding energy and broadening of the Cu $2p_{3/2}$ peak can be observed. This phenomenon indicates the existence of at least two kinds of surface copper species that differ in their chemical environments. Deconvolution of the original Cu $2p_{3/2}$ peaks was thus carried out and the peak positions as well as their contributions extracted from the deconvolution are listed in Table 2. The species with binding energies between 934.0 and 934.2 eV as measured for CZ-550, CZ-650, and CZ-750 are attributable to bulk CuO.[5,9] The binding energies of the other species are about 2 eV lower, which may be corresponding to the copper oxide located near the oxygen vacancies on the surface of zirconia support as proposed above.

The XPS intensity ratio of Cu 2p/Zr 3d values for various CuO/ZrO_2 catalysts is also included in Table 2, which reflects the copper dispersion on zirconia support. The surface atomic ratio of Cu/Zr increases with the increase of calcination temperature with a maxima at 550 °C and then decreases with further increase of calcination temperature. Except in the case of the CZ-550 sample, the Cu/Zr ratio is falling in the range of 0.336−0.47 for most of the materials. These values are smaller than the ratio (∼0.5) as used for the bulk phase, inferring that a preferential accumulation of the Zr-components occurs during the course of the catalyst preparation. A significant higher value of 0.56 is observed for the CZ-550 sample, thus pointing to a pronounced Cu enrichment on the surface. The activity of the catalysts in the steam reforming of methanol was also found to increase up to calcination at 550 °C and decreases with further increase of calcination temperature. As shown in Section 3.1, a much higher dispersion of copper oxide on ZrO_2 is also noticed for sample CZ-550 by the N_2O titration method. Thus, the present XPS results are in good agreement with the dispersion of copper determined by N_2O titration method.

In situ FTIR CO adsorption analysis is another powerful technique for the study of the chemical states of copper species,[58] especially for the identification of oxidation state of copper species deposited on the surface of metal oxides. Figure 5 shows the in situ DRIFT spectra of CO adsorption of various Cu/ZrO_2 catalysts after reduction pretreatment as described in Section 3.1. Adsorption of CO on sample CZ-350 results in the evolution of one band at 2108 cm^{-1}, which is red-shifted to 2105 and 2102 cm^{-1} for CZ-450 and CZ-550, and back to a higher frequencies of 2107 and 2110 cm^{-1} for CZ-650 and CZ-750 samples, respectively. This band is assigned to Cu^0-CO species,[58] the shift of which may be caused by the structural and electronic changes of copper, as proposed by De Jong et al..[59] Worth mentioning is that the CZ-550 catalyst showed the maximum CO absorbance at ca. 2100 cm^{-1}, in excellent agreement with the N_2O titration and XPS data that sample calcined at 550 °C has the highest surface copper dispersion. In addition, a new weak band at 2013 cm^{-1} is registered for sample CZ-550 and continuously shifted to lower frequencies for higher temperature calcined samples. According to the literature,[60] this band is associated with the carbonyls linearly adsorbed on the Cu^0 atoms with significantly lower coordination number. The shift toward lower frequencies can be explained by the presence of larger copper particles in the catalysts calcined at higher temperatures, which could donate more electron density to the carbon-copper bond.

To investigate the reducibility of the copper species in various CuO/ZrO_2 calcined catalysts, TPR measurements were carried out and reported in Figure 6. All the samples exhibit a broad reduction profile together with shoulders in the temperature

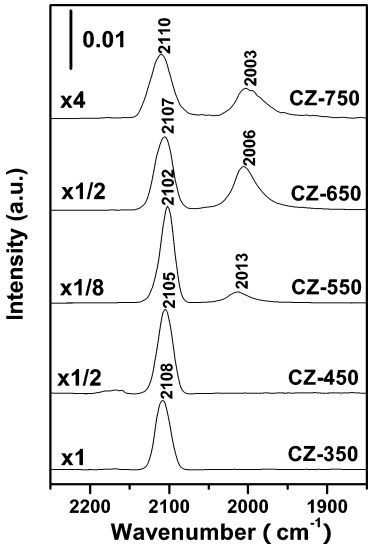

Figure 5. In situ DRIFT spectra of CO adsorption on Cu/ZrO_2 catalysts as a function of calcination temperature.

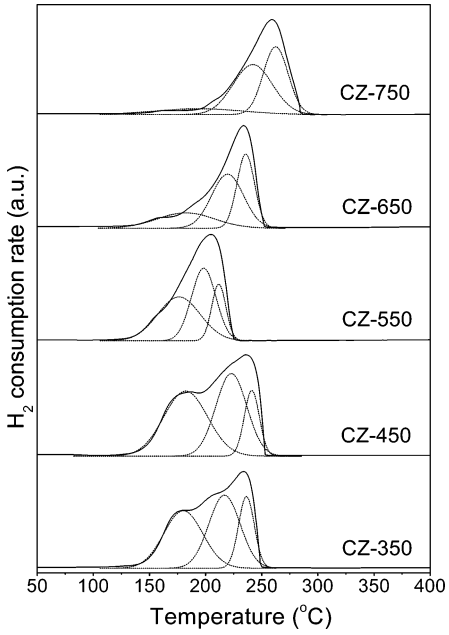

Figure 6. TPR profiles of various CuO/ZrO_2 catalysts.

TABLE 3: TPR-Fitting Results of Cu/ZrO_2 Catalysts Calcined at Different Temperatures

	T_M (°C)			proportion of total area (%)		
sample	α	β	γ	α	β	γ
CZ-350	180	217	236	24.5	35.2	40.2
CZ-450	182	223	241	33.2	30.8	35.9
CZ-550	176	198	212	22.2	63.4	14.4
CZ-650	182	220	236	11.9	32.5	55.6
CZ-750	194	242	262	6.1	30.2	63.6

range 200−300 °C. Previously, it is shown that the reduction of bulk CuO is featured by a single reduction peak at a considerably higher temperature of 320 °C.[47] It is thus concluded that there is a pronounced Cu/Zr interaction which facilitates the reduction of the supported copper species. As the calcination temperature increases, the main reduction peak becomes narrower and shifts to lower temperature. In order to gain a further insight into the TPR results, the profiles are deconvoluted using a computer program.[47] The peak positions and their contributions derived from deconvolution are summarized in Table 3. The original TPR profiles can be deconvoluted into at least three peaks in all cases. This suggests the presence of at least three different types of CuO phase in the Cu/ZrO_2 samples, where highly dispersed CuO phase (α-peak), crystallized copper oxide strongly (β-peak) or weakly (γ-peak) interacted with the ZrO_2 surface coexist.[61] Such multiple TPR peaks have also been noticed by Takezawa et al.[62] and Liu et al.[63] They have attributed the low-temperature reduction peak to highly dispersed copper(II) ions in an octahedral environment.[62,63] As can be seen from Table 2, the fraction of lower temperature reduction peaks, that is, the α- and β-peaks, is found to be the highest and shifts to lower temperatures for sample CZ-550 as compared to other samples, indicating the presence of a stronger Cu−Zr interaction in the sample prepared by calcination at 550 °C.

3.3. Catalytic Steam Reforming of Methanol. The catalytic activity, selectivity, and stability of the present nanostructured Cu/ZrO_2 catalysts are tested for the steam reforming of methanol, which represents a promising alternative for use in catalytic generation of high purity H_2 to produce clean electrical energy from fuel cells for vehicles applications.[5,9,11] Figure 7 shows a typical set of results for methanol steam reforming over the CZ-550 catalyst, illustrating the effect of temperature on the methanol conversion and the molar compositions with respect to carbon dioxide, hydrogen, and carbon monoxide. As shown, the methanol conversion exhibits a typical S-shaped temperature dependence.[5] H_2 and CO_2 are produced approximately in a 3:1 ratio, and substantial CO formation is initiated at around 280 °C, when conversion of methanol approaches completeness. Additional experiments, as reported in a previous paper from our laboratory,[47] indicated that CO was not formed at short contact times and that its concentration only became significant when the methanol was almost completely consumed at longer contact times. Also, as demonstrated previously[47] when compared to the catalysts prepared by conventional methods, the oxalate gel-coprecipitation derived Cu/ZrO_2 catalyst shows enhanced activity and long-term stability in methanol steam reforming.

The catalytic activity and selectivity of the various Cu/ZrO_2 catalysts measured at 260 °C in the steam reforming of methanol are illustrated in Figure 8. In all cases, H_2 and CO_2 were detected as the major component in the effluent gas, together with a minor amount of CO. No other products, such as dimethyl ether, methyl formate, and methane, could be detected over any of the catalysts tested. It can be seen that the activity of the Cu/ZrO_2 catalyst was enhanced monotonously by increasing the

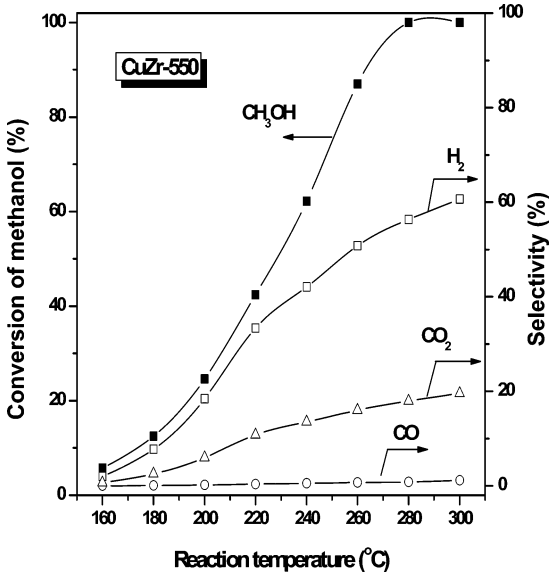

Figure 7. Product gas composition and methanol conversion vs reaction temperature during steam reforming of methanol over catalyst CZ-550. (Reaction conditions: $H_2O/CH_3OH = 1.3$ molar ratio, WHSV = 5.4 h^{-1}, $p = 0.1$ MPa).

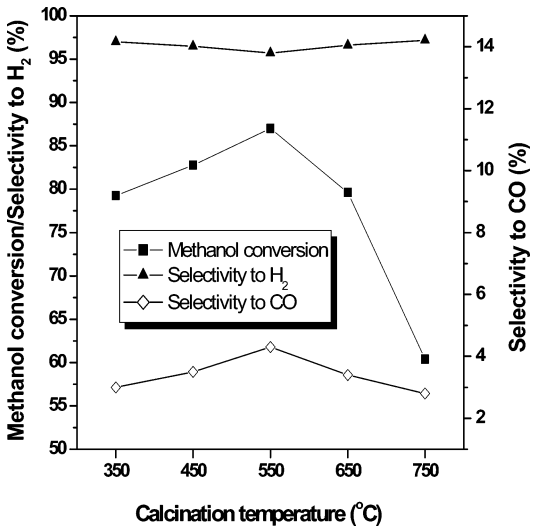

Figure 8. Catalytic performance of various Cu/ZrO_2 catalysts. (Reaction conditions: $H_2O/CH_3OH = 1.3$ molar ratio, WHSV = 5.4 h^{-1}, $p = 0.1$ MPa, 260 °C).

calcination temperature and reached a maximum at 550 °C. Further increase of the calcination temperature led to a rapid decrease of the activity. The selectivity to CO increased with the calcination temperature until 550 °C and then rapidly decreased for higher temperature calcined samples. Moreover, an opposite trend for the selectivity toward the formation of H_2 as a function of calcination temperature is identified. This indicates that it is difficult to suppress CO evolution at high-methanol conversion region due to the presence of reverse water gas shift reaction

$$CO_2 + H_2 \rightarrow CO + H_2O \quad (1)$$

as a consecutive reaction of methanol steam reforming (SRM)[5,8]

$$CH_3OH + H_2O \rightarrow CO_2 + 3H_2 \quad (2)$$

at a higher conversion levels.

4. Discussions

Results obtained in this study clearly demonstrate that the structural evolution of zirconia in the Cu/ZrO_2 system, which varies with respect to the calcination temperatures, plays a key role in determining the physicochemical and catalytic properties of the final materials. Zirconia has attracted considerable recent attention as both a catalyst and a catalyst support because of its high thermal stability and the amphoteric character of its surface hydroxyl groups.[38−40] When zirconia is used as a support, various reactions such as Fischer−Tropsch synthesis, hydrodesulfurization, and methanol synthesis have been reported to proceed with higher rates and selectivity than with other supports.[22−27] In the specific field of methanol chemistry, it is expected that new improved Cu/ZrO_2 catalyst system with enhanced methanol synthesis rates may be rationally optimized by tailoring the structural distribution of ZrO_2 among amorphous, tetragonal, and monoclinic phases.[38−40] In the present work, we have unambiguously demonstrated that in addition to the phase constitution, the specific microstructural arrangement of the respective zirconia phases appears to be the key factor that controls the catalytic performance of the Cu/ZrO_2 system. Noteworthy is that the 500 °C calcined Cu/ZrO_2 catalyst featured with the tetragonal ZrO_2 as the major crystalline phase and monoclinic ZrO_2 as the main surface layer of the support exhibits enhanced catalytic performance in terms of methanol conversion or H_2 production rate as compared to other samples. These findings form new basis for the structure−activity relationships of the copper catalysts in methanol chemistry, which are prerequisites for a knowledge-based design of improved catalytic materials.

The structural evolution followed by XRD and visible Raman spectroscopy has revealed that the phase transformation of ZrO_2 in the present copper−zirconia system follows the sequence of amorphous → tetragonal → monoclinic over 350−750 °C. The XRD results show that the phase transformation from tetragonal to monoclinic phase began at 650 °C and completed at 750 °C. Meanwhile, the Raman data demonstrate that the phase change of tetragonal starts already at 550 °C, which indicates that the phase transformation of zirconia from tetragonal to monoclinic takes place initially at the surface regions of the $Cu−ZrO_2$ sample. Such significant surface structural rearrangement is also corroborated by XPS analysis, as inferred by the appreciable formation of surface anionic defects associated with the creation of Zr^{3+} species on the surface of the 550 °C calcined material. Recently, by taking the unique advantage of the surface-sensitive nature of the UV Raman technique, Li and his co-workers have shown that upon calcination the phase change from tetragonal to monoclinic ZrO_2 begins at the surface region and then extends into the bulk until the whole particle changes into the monoclinic phase.[64] Later, the same authors also revealed that the tetragonal to monoclinic phase transformation initiates at 400 °C, and the phase totally becomes monoclinic at about 700 °C.[64] A closer comparison of the XRD and visible Raman data reported herein with the XRD and UV Raman data by Li et al.[64] indicates that the tetragonal to monoclinic phase transformation requires a higher temperature for present Cu/ZrO_2 system than for pure ZrO_2, inferring a pronounced copper-induced stabilization of the metastable tetragonal structure in the surface region.

With regard to the essential nature of zirconia phase as the support of copper catalysts for methanol synthesis or SRM reaction, the crystalline structure of ZrO_2 has recently been established as one of the main factors for rationalization of the structure−activity relationships of Cu-based catalysts.[38−42] Very recently, on investigating the effect of ZrO_2 phase on the catalytic performance of a series of impregnation-derived Cu/ZrO_2 catalysts, Bell et al. disclosed that the Cu catalysts deposited on m-ZrO_2 are nearly an order of magnitude more active for methanol synthesis than their analogues prepared with t-ZrO_2.[38,39] The reason of this effect has been rationalized as the higher CO adsorption capacity of m-ZrO_2 as a consequence of its higher concentration of surface anionic vacancies. It is also believed that the phase transformation from tetragonal to monoclinic phase can entail a geometric effect that can influence the dispersion, leading to change in the morphology of the supported copper metal particles as well as enhanced metal−support interaction and reinforced synergy between Cu and ZrO_2.[38,39] At this situation, it is important to note that the XPS results show that the phase change from tetragonal to monoclinic phase, even merely in the surface regions of ZrO_2, can allow the generation of higher amount of surface anionic vacancies in the present Cu/ZrO_2 system. Taking into account all these structural features rendered by the different ZrO_2 polymorphs, it is reasonable that the structural rearrangement, in particular in the surface regions of zirconia, is found to play a significant role in controlling the size, and dispersion of the active copper phase, as well as the metal−support interaction in the present Cu/ZrO_2 system (see Figure 9).

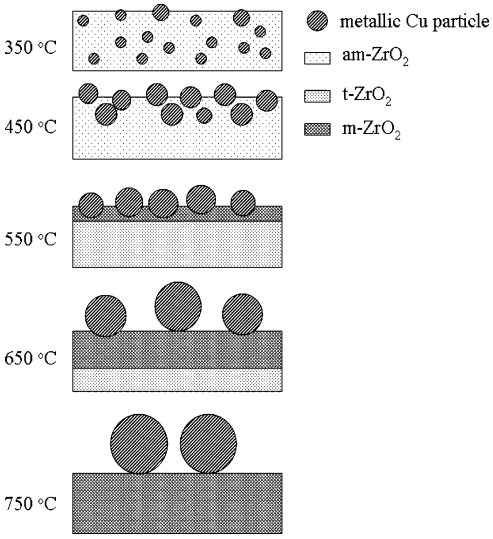

Figure 9. Schematic illustration of the structural evolution of the nanostructured Cu/ZrO_2 catalyst as a function of precursor calcination.

Investigation by means of TPR, N_2O titration, and XPS combined with CO-adsorption has confirmed that the 550 °C calcined material featured with the monoclinic ZrO_2 as the dominant surface layer of the support exhibits enhanced copper surface area, stronger metal−support interaction and hence improved SRM activities as compared to other samples. Nevertheless, XRD and N_2 adsorption measurements have confirmed that with the calcination temperature increasing from 350 to 750 °C a continuous increase in the copper particles size and loss of the BET specific surface area occurs. This indicates that N_2O titration is a better method for measuring the dispersion of Cu on zirconia. Most likely, the evolution of surface copper dispersion is affected by two competitive factors. On one hand, the crystallization of the amorphous ZrO_2 upon higher calcination temperature leads to the segregation of CuO particles from the ZrO_2 matrix and increase of higher accessible copper surface area, as evidenced by the decreasing deviations of S_{Cu}^{XRD} from $S_{Cu}^{N_2O}$ values (see Table 1). On the other hand, the growth of copper particle size leads to the decrease of copper metal surface area. When the catalyst was calcined below 550 °C, the growth

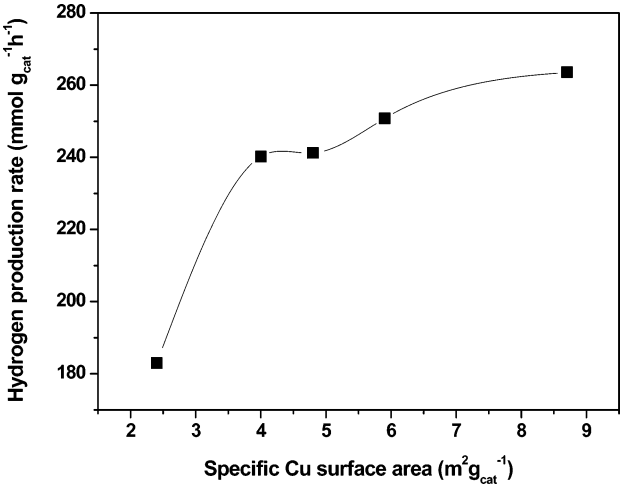

Figure 10. The relationship between the measured specific Cu surface area (S_{Cu}, $m^2 \cdot g^{-1}$) and hydrogen-production rate (R_{H_2}, mmol $gcat^{-1}$ h^{-1}) at 260 °C.

of copper particle size is limited because of the stabilizing effect of ZrO_2, while the exposure of copper surface induced by the crystallization of ZrO_2 is more significant. Above 550 °C, the growth of CuO particle size plays a predominant role in the structural change of Cu/ZrO_2 catalyst, which also weakens the interaction between copper and zirconia and consequently deteriorates the catalytic activity.

At this juncture, it is interesting to note that metallic copper surface area has widely been assumed to be the main parameter for the structure−activity correlation of Cu-based catalysts, given the well-established role of Cu as the main active component for methanol synthesis or related processes.[44,45] However, there are also conflicting reports that suggest that the methanol conversion or hydrogen production rate does not show correlation with the surface area of metallic copper for the Cu-based catalysts.[10,,65] For instance, instead of the observation of a positive correlation of the enhanced activity with the increasing copper surface area, Ressler et al. have recently identified an excellent linear relationship between the SRM activity and the lattice microstrain values of the Cu nanoparticles embedded in the matrix of zinc oxide.[10,66,67] It is therefore worthwhile to make a comparison between the catalytic activity of the present Cu/ZrO_2 catalysts and the specific copper surface area as determined by surface titration with N_2O. Figure 10 shows the effect of the surface area of metallic copper on the hydrogen production rate (R_{H_2}) from methanol steam reforming over the various Cu/ZrO_2 catalysts obtained by gel-coprecipitation of oxalate precursors. Apparently, the increase in H_2 production rates does not show linear correlation with the increasing copper surface area for the five copper−zirconia catalysts. This demonstrates that although a high Cu surface area is a prerequisite for catalytic activity, it does not account for the observed activity changes alone without taking the powerful synergy between copper and zirconia into account.

Although the main purpose of this paper was to present a detailed investigation of the structural evolution of the respective Cu and ZrO_2 phases occurring in the Cu/ZrO_2 catalyst systems upon calcination at elevated temperatures, we would like to comment here on the practical consequences of the present results. Aqueous precipitation or sol−gel methods are often employed to produce various zirconia-based functional materials.[68] In most cases, the initial product is an amorphous zirconium oxyhydroxide or a mixture of a-ZrO_2 and t-ZrO_2. Calcination of the initial product at progressively higher temperatures leads to the conversion of all of the a-ZrO_2 to t-ZrO_2, and at higher temperatures to the conversion of t-ZrO_2 to m-ZrO_2.[68] Because treatments also lead to a decrease in surface area, m-ZrO_2 is usually obtained with much lower surface area than t-ZrO_2.[57,68] While it is not yet possible to achieve a complete tetragonal to monoclinic transformation at lower temperatures, results obtained in this study indicate that a minor portion of the t-ZrO_2 in the surface region can be effectively transformed to a pure monoclinic phase without significant loss in surface area. The net result is that high surface area ZrO_2 supports with the properties of pure m-ZrO_2 can be obtained by thermal treatment of t-ZrO_2 under moderate conditions. This highlights new opportunities in the development of highly active and selective zirconia-based catalysts for a wide range of catalytic reactions.

5. Conclusions

This study demonstrates that the precursor calcination markedly affects the structure, reducibility, and dispersion of Cu/ZrO_2 catalysts. The XRD results presented in this paper indicate that the phase transformation of zirconia from tetragonal to monoclinic requires a calcination temperature of 650 °C. Nevertheless, Raman and XPS spectroscopies reveal that the formation of monoclinic phase zirconia occurs already at the near surface regions of the 550 °C calcined sample. As opposed to the in situ XRD bulk analysis, N_2O titration is found to be a more valuable method for measuring the dispersion of Cu on ZrO_2. The results of N_2O titration suggest that copper dispersion depends highly on the surface and structural nature of the ZrO_2 support. The information obtained by TPR reveals the presence of three types of copper species on the ZrO_2 support. The dispersion of Cu as determined by N_2O titration corroborates the findings of XPS and in situ DRIFTS of CO adsorption. The catalytic activity of the Cu/ZrO_2 catalysts for the steam reforming of methanol also finds direct correlation with the dispersion with the catalyst featured with surface-enriched monoclinic phase being the most active for this reaction.

Acknowledgment. This work was supported by the National Natural Science Foundation of China (Grants 20421303, 20473021, 20633030), the National Basic Research Program of China (Grant 2003CB615807), the National High Technology Research and Development Program of China (Grant 2006AA03Z336), the Committee of the Shanghai Education (Grant 6SG03), and the Research Fund for the Doctoral Program of Higher Education (Grant 20050246071).

References and Notes

(1) Praliaud, H.; Mikhailenko, S.; Chajar, Z.; Primet, M. *Appl. Catal., B* **1998**, *16*, 359.
(2) Radtke, F.; Koeppel, R. A.; Minardi, E. G.; Baiker, A. *J. Catal.* **1997**, *167*, 127.
(3) Ko, J. B.; Bae, C. M.; Jung, Y. S.; Kim, D. H. *Catal. Lett.* **2005**, *105*, 157.
(4) Yahiro, H.; Nakaya, K.; Yamamoto, T.; Saiki, K.; Yamaura, H. *Catal. Commun.* **2006**, *7*, 228.
(5) Agrell, J.; Birgersson, H.; Boutonnet, M.; Melian-Cabrera, I.; Navarro, R. M.; Fierro, J. L. G. *J. Catal.* **2003**, *219*, 389.
(6) Kim, T. W.; Song, M. W.; Koh, H. L.; Kim, K. L. *Appl. Catal., A* **2001**, *210*, 35.
(7) Ma, Z-Y.; Yang, C.; Wei, W.; Li, W.-H.; Sun, Y.-H. *J. Mol. Catal., A* **2005**, *231*, 75.
(8) Breen, J. P.; Ross, J. R. H. *Catal. Today* **1999**, *51*, 521.
(9) Matter, P. H.; Braden, D. J.; Ozkan U. S. *J. Catal.* **2004**, *223*, 340.
(10) Kniep, B. L.; Ressler, T.; Rabis, A.; Girgsdies, F.; Baenitz, M.; Steglich, F.; Schlogl, R. *Angew. Chem., Int. Ed.* **2004**, *43*, 112.
(11) Velu, S.; Suzuki, K.; Okazaki, M.; Kapoor, M. P.; Osaki, T.; Ohashi, F. *J. Catal.* **2000**, *194*, 373.

(12) Saadi, A.; Rassoul, Z.; Bettahar, M. M. *J. Mol. Catal. A* **2000**, *164*, 205.
(13) Rao, R.; Dandekar, A.; Baker, R. T. K.; Vannice, M. A. *J. Catal.* **1997**, *171*, 406.
(14) Chary, K. V. R.; Sagar, G. V.; Srikanth, C. S.; Rao, V. V. *J. Phys. Chem. B* **2007**, *111*, 543.
(15) Fabina, M. T.; Schmal, M. *Appl. Catal., A* **1997**, *163*, 153.
(16) Fridman, V. Z.; Davydov, A. A. *J. Catal.* **2000**, *195*, 20.
(17) Chen, K.; Xie, S.; Iglesia, E.; Bell, A. T. *J. Catal.* **2000**, *189*, 421.
(18) Ortelli, E. E.; Wambach, J.; Wokaun, A. *Appl. Catal., A* **2001**, *216*, 227.
(19) Tanabe, K.; Yamaguchi, T. *Catal. Today* **1994**, *20*, 185.
(20) Yamaguchi, T. *Catal. Today* **1994**, *20*, 199.
(21) Vrinat, M.; Hamon, D.; Breysse, M.; Durand, B.; Des Courrieres, T. *Catal. Today* **1994**, *20*, 273.
(22) Fisher, I. A.; Bell, A. T. *J. Catal.* **1997**, *172*, 222.
(23) Arena, F.; Barbera, K.; Italiano, G.; Bonura, G.; Spadaro, L.; Frusteri, F. *J. Catal.* **2007**, *249*, 185.
(24) Lisitsyn, A. S.; Kuznetsov, V. L.; Yermakov, Y. I. *React. Kinet. Catal. Lett.* **1980**, *14*, 445.
(25) Bruce, L. A.; Hope, G. H.; Matthews, J. F. *Appl. Catal.* **1983**, *8*, 349.
(26) Miyata, H.; Tokuda, S.; Ono, T.; Ohno, T.; Hatayama, F. *J. Chem. Soc., Faraday Trans.* **1990**, *86*, 2291.
(27) Kulkarni, D.; Waches, I. E. *Appl. Catal., A* **2002**, *237*, 121.
(28) Cubeiro, M. L.; Fierro, J. L. G. *Appl. Catal., A* **1998**, *168*, 307.
(29) Burcham, L. J.; Waches, I. E. *Catal. Today* **1999**, *49*, 467.
(30) Ilyas, M.; Ikramullah. *Catal. Commun.* **2004**, *5*, 1.
(31) Koppel, R. A.; Stocker, C.; Baiker, A. *J. Catal.* **1998**, *179*, 515.
(32) Ritzkopf, I.; Vukojević, S.; Weidenthaler, C.; Grunwaldt, J.; Schüth, F. *Appl. Catal., A* **2006**, *302*, 215.
(33) Bartley, G. J. J.; Burch, R. *Appl. Catal., A* **1988**, *43*, 141.
(34) Saito, M.; Fujitani, T.; Takeuchi, M.; Watanabe, T. *Appl. Catal., A* **1996**, *138*, 311.
(35) Frank, B.; Jentoft, F. C.; Soerijanto, H.; Kröhnert, J.; Schlögl, R.; Schomäcker, R. *J. Catal.* **2007**, *246*, 177.
(36) Jung, K. T.; Bell, A. T. *Catal. Lett.* **2002**, *80*, 63.
(37) Rhodes, M. D.; Bell, A. T. *J. Catal.* **2005**, *233*, 198.
(38) Rhodes, M. D.; Pokrovski, K. A.; Bell, A. T. *J. Catal.* **2005**, *233*, 210.
(39) Zhao, Y.; Tao, K.; Wan, H. L. *Catal. Commun.* **2004**, *5*, 249.
(40) Ma, Z. Y.; Yang, C.; Wei, W.; Li, W. H.; Sun, Y. H. *J. Mol. Catal. A* **2005**, *231*, 75.
(41) Koeppel, R. A.; Baiker, A.; Wokaun, A. *Appl. Catal., A* **1992**, *84*, 77.
(42) Chinchen, G. C.; Waugh, K. C.; Whan, D. A. *Appl. Catal.* **1986**, *25*, 101.
(43) Kurtz, M., Wilmer, H.; Genger, T.; Hinrichsen, O.; Muhler, M. *Catal. Lett.* **2003**, *86*, *77*.
(44) Chang, S.; Doong, R. *Chem. Mater.* **2005**, *17*, 4837.
(45) Muñoz, M. C.; Gallego, S.; Beltrán, J. I.; Cerdá, J. *Surf. Sci. Rep.* **2006**, *61*, 303.
(46) Zhang, X. R.; Wang, L. C.; Yao, C. Z.; Cao, Y.; Dai, W. L.; He, H. Y.; Fan, K. N. *Catal. Lett.* **2005**, *102*, 183.
(47) Yao, C. Z.; Wang, L. C.; Liu, Y. M.; Wu, G. S.; Cao, Y.; Dai, W. L.; He, H. Y.; Fan, K. N. *Appl. Catal., A* **2006**, *297*, 151.
(48) Porter, D. L.; Heuer, A. H. *J. Am. Ceram. Soc.* **1979**, *62*, 298.
(49) Deng, J. F.; Sun, Q.; Zhang, Y. L.; Chen, S. Y.; Wu, D. *Appl. Catal., A* **1996**, *139*, 75.
(50) Chinchen, G. C.; Hay, C. M.; Vandervell, H. D.; Waugh, K. C. *J. Catal.* **1987**, *103*, 79.
(51) Wang, Y.; Caruso, R. A. *J. Mater. Chem.* **2002**, *12*, 1442.
(52) Wu, G. S.; Sun, Y. H.; Li, Y. W.; Jiao, H.; Xiang, H. W.; Li, Y. Y. *J. Mol. Struct.* **2003**, *626*, 287.
(53) Wang, L. C.; Liu, Y. M.; Chen, M.; Cao, Y.; He, H. Y.; Wu, G. S.; Dai, W. L.; Fan, K. N. *J. Catal.* **2007**, *246*, 193.
(54) Xie, S.; Iglesia, E.; Bell, A. T. *Chem. Mater.* **2000**, *12*, 2442.
(55) Luo, M. F.; Fang, P.; He, M.; Xie, Y. L. *J. Mol. Catal. A* **2005**, *239*, 243.
(56) Ardizzone, S.; Bianchi, C. L. *Surf. Interface Anal.* **2000**, *30*, 77.
(57) Velu, S.; Suzuki, K.; Gopinath, C. S.; Yoshidac, H.; Hattori, T. *Phys. Chem. Chem. Phys.* **2002**, *4*, 1990.
(58) Dandekar, A.; Vannice, M. A. *J. Catal.* **1998**, *178*, 621.
(59) de Jong, K. P.; Geus, J. W.; Joziasse, J. *Appl. Surf. Sci.* **1980**, *6*, 273.
(60) Hadjiivanov, K.; Venkov, T.; Knözinger, H. *Catal. Lett.* **2001**, *75*, 55.
(61) Słoczyński, J.; Grabowski, R.; Kozłowska, A.; Olszewski, P. K.; Stoch, J. *Phys. Chem. Chem. Phys.* **2003**, *5*, 4631.
(62) Shimokawabe, M.; Asakawa, H.; Takezawa, N. *Appl. Catal.* **1990**, *59*, 45.
(63) Liu, J.; Shi, J.; He, D.; Zhang, Q.; Wu, X.; Liang, Y.; Zhu, Q. *Appl. Catal., A* **2001**, *218*, 113.
(64) Li, M.; Feng, Z.; Xiong, G.; Ying, P.; Xin, Q.; Li, C. *J. Phys. Chem. B* **2001**, *105*, 8107.
(65) Zhang, X. R.; Wang, L. C.; Cao, Y.; Dai, W. L.; He, H. Y.; Fan, K. N. *Chem. Commun.* **2005**, 4104.
(66) Gunter, M. M.; Ressler, T.; Jentoft, R. E.; Bems, B. *J. Catal.* **2001**, *203*, 133.
(67) Gunter, M. M.; Ressler, T.; Bems, B.; Buscher, C.; Genger, T.; Hinrichsen, O.; Muhler, M.; Schlogl, R. *Catal. Lett.* **2001**, *71*, 37.
(68) Tyagi, B.; Sidhpuria, K.; Shaik, B.; Jasra, R. V. *Ind. Eng. Chem. Res.* **2006**, *45*, 8643.